Diverse electron and ion acceleration characteristics observed over Jupiter's main aurora

B. H. Mauk[1], D. K. Haggerty[1], C. P. Paranicas[1], G. Clark[1], P. Kollmann[1], A. M. Rymer[1], J. M. Peachey[1], S. J. Bolton[2], S. M. Levin[3], A. Adriani[4], F. Allegrini[2,5], F. Bagenal[6], B. Bonfond[7], J. E. P. Connerney[8], R. W. Ebert[2], G. R. Gladstone[2], W. S. Kurth[9], D. J. McComas[10,2], D. Ranquist[6], P. Valek[2]

1. The Johns Hopkins University Applied Physics Laboratory, Laurel, Maryland, USA (Barry.Mauk@jhuapl.edu)
2. Southwest Research Institute, San Antonio, Texas, USA
3. Jet Propulsion Laboratory, Pasadena, California, USA
4. Instituto Nazionale di Astrofisica-Instituo di Astofisica e Planetologia Spaziali, Roma, Italy
5. Physics and Astronomy Department, University of Texas at San Antonio, Texas, USA
6. University of Colorado, Boulder, Colorado, USA
7. Université de Liège, Technologies and Astrophys. Res. Institute, LPAP,, Liège, Belgium
8. NASA Goddard Space Flight Center, Greenbelt, Maryland, USA
9. University of Iowa, Iowa City, Iowa, USA
10. Department of Astrophysical Sciences, Princeton University, Princeton, New Jersey, USA

This article has been accepted for publication and undergone full peer review but has not been through the copyediting, typesetting, pagination and proofreading process which may lead to differences between this version and the Version of Record. Please cite this article as doi: 10.1002/2017GL076901

Abstract. Two new Juno-observed particle features of Jupiter's main aurora demonstrate substantial diversity of processes generating Jupiter's mysterious auroral emissions. It was previously speculated that sometimes-observed potential-driven aurora (up to 400 kV) can turn into broadband stochastic acceleration (dominating at Jupiter) by means of instability. Here direct evidence for such a process is revealed with a "mono-energetic" electron inverted-V rising in energy to 200 keV, transforming into a region of broadband acceleration with downward energy fluxes tripling to 3000 mW/m^2, and then transforming back into a mono-energetic structure ramping down from 200 keV. But a second feature of interest observed nearby is unlikely to have operated in the same way. Here a downward accelerated proton inverted-V, with inferred potentials to 300-400 kV, occurred simultaneously with downward accelerated broadband electrons with downward energy fluxes as high as any observed (~3000 mW/m^2). This latter feature has no known precedent with Earth auroral observations.

1. Introduction

Jupiter's uniquely powerful auroras are highly puzzling when compared to Earth auroras. Initial observations from NASA's Juno mission (Allegrini et al., 2017; Connerney et al., 2017a; Mauk et al., 2017a) showed none of the expected peaked electron distributions that would be indicative of magnetic field-aligned electric potentials (see Bolton et al. 2017a; 2017b; and Bagenal et al. 2017 for more information about Juno). Magnetic perturbations associated with anticipated magnetic field-aligned electric currents were far weaker than expected (Connerney et al., 2017a). Subsequent observations did identify peaked electron distributions over the main aurora, indicative of magnetic field-aligned electric potentials as high as 400 kV, but they delivered less electron energy flux to the aurora than broadband processes acting nearby with energies exceeding 1 MeV (Mauk et al., 2017b).

For the study showing peaked electron distributions (Mauk et al. 2017b), there was a hint of an evolution from a strongly peaked distribution, to a distribution that seemed to combine coherent and broadband acceleration, to a distribution with only broadband acceleration characteristics and with the strongest downward energy fluxes. These three regions, while closely spaced in time, were not simply connected; there were lower intensity regions between them. It was speculated that as the power density of potential-driven auroras becomes higher, some instability initiates that yields stronger acceleration through some stochastic process.

The present study further emphasizes the importance of broadband acceleration processes with two distinct new features observed during a pass over Jupiter's northern main aurora on 11 July 2017 (Juno's 7th perijove, PJ7). The particle data reported here were obtained by the Jupiter Energetic particle Detector Instrument (JEDI; Mauk et al., 2017c).

2. Previous observations

Figure 1 shows a previously reported observation (Mauk et al. 2017b) of inverted-V electron distributions. Qualitative auroral context is provided in Figure 2A using Juno's UVS imager (Gladstone et al., 2017). Proton distributions are added in panels 1E and 1F to the previously published figure. Here, in association with the downward accelerated inverted-V electron distribution in panel 1C is an upward proton angular beam (panels 1E and 1F; pitch angle distributions are derived with help from Juno's magnetometer; Connerney et al., 2017b). The highly directional proton distributions (beaming in angle) are broad in energy, showing only a couple of isolated distributions with energy peaks (see later discussion). As previously reported, the downward energy fluxes associated with the electron inverted-V (Panel 1B) are smaller than the peak energy fluxes observed during other main-aurora crossings, and smaller than the peak energy fluxes observed nearby, where the distributions

are broadband. Note was previously taken of the transition from spectrum 2 in panel 1A, through spectrum "3" which seems to combine elements of coherent and broadband acceleration, to spectrum "4" with strictly broadband characteristics. The hypothesis that this evolution occurred as a result of an instability of strong potential-driven aurora was pure speculation; Figure 1 does not provide any particularly powerful evidence for such an occurrence.

It is interesting to note differences between Earth and Jupiter auroral observations (see Pashmann et al., 2002 or Amm et al., 2002 for Earth aurora reviews). To note just one example, while the jovian inverted-V signatures look similar to Earth's, the associated electron distributions at Jupiter are often more narrowly confined to the downward direction, contrary to the typically more angularly isotropic distributions observed at Earth (although counter examples exist; Arnoldy, 1981).

3. New observations

Both new features discussed here are shown in Figure 3, comprising the proton inverted-V signature on the left, centered near 01:14:38 (panel 3G) and the electron inverted-V signature on the right, centered near 01:15:52 (panel 3C). Figure 2B provides qualitative auroral context for the in situ observations. Juno was flying at low altitude over Jupiter's main aurora in the northern hemisphere (on 11 July 2017). Two estimates of the magnetic mapping from Juno to the auroras are shown, and yellow rectangles on the trajectories show the time period of Figure 3. There are substantial azimuthal gradients in auroral intensity, and so the uncertainties in magnetic mapping (Methods section of Mauk et al., 2017b) make it impossible to know which auroral features correspond to the new particle features of interest here (a subject of future studies). The images show piecewise snapshots in time, and the jovian aurora can be quite time variable (Gladstone et al., 2017; Bonfond et al., 2017).

Before discussing our focus features, we note some peculiar aspects of the electron measurements. In panel 3C there is a horizontal band centered at about 160 keV. It corresponds to the fraction of higher energy electrons, beginning at about 400 keV, that fully penetrate the 0.5 mm solid state detectors (SSDs) and leave behind a "minimum ionizing" feature. These are primarily foreground electrons (having reached the detector through the collimator) and are not (mostly) the >15 MeV electrons that reach the detector through the instrument housing (Paranicas et al., 2017). We have developed procedures for correcting for the penetrator features for individual spectra (Supporting Information S1). The calculation of the energy flux in panel 3A uses both uncorrected spectra (black lines, representing lower limits) and partially corrected spectra (red lines, representing upper limits; Supporting Information S2). In principal the minimum ionizing feature might be confused with features associated with coherent auroral acceleration. It turns out that sharply peaked auroral acceleration is rarely accompanied by the high energy tails that result in the minimum ionizing feature; our procedures cleanly separate the two phenomena (Supporting Information S3).

An additional caveat to the electron data are the features identified with the green bars at the top of panel 3A. Here the electron intensities have become so high that the JEDI sensors are partially saturated. A quantitative procedure for identifying these regions is presented in the Supporting Information S4. What is clear in these cases is that the high energy tails have become unambiguously very hard (the intensities at the higher energies have increased and do not fall off rapidly as a function of energy).

4. Downward electron inverted-V

The first feature of interest is the electron inverted-V (panel 3C) centered near 01:15:52 UT on the figure's right side. We zoom in on this feature in Figure 4. What is

interesting here is that the inverted-V appears to have evolved into a broadband acceleration region near the 200 keV peak of the V-structure. And, just like we saw before, the maximum downward electron energy fluxes occur within that broadband acceleration region. The downward going electrons in both the inverted-V and broadband regions (~120°-180° pitch angles in panel 3B) appear to be reflected or scattered back upward (<~ 60° pitch angles) but with a substantial fraction of electrons within the loss cone being lost. The loss cone is crudely estimated at ~28° using the simple expression in Mauk et al. (1917a). Such electron loss-cone features are sometimes observed (Figure 1), and sometimes not observed (left side of Figure 3; see also Mauk et al., 1917a) in more general broadband acceleration regions.

Downward electron spectra from this period are shown in panels 5-8 in Figure 5, corrected where needed as discussed in the Supporting Information S1. The time position for each spectrum is shown at the bottom of panel 4A. We have here in Figure 4 sudden transitions between coherent and the broadband acceleration without any apparent gaps. Because the electron distributions in the center region are partially saturated, it is possible that a peaked auroral acceleration feature is hidden within the smeared features observed at intermediate energies. But the high energy tails have unambiguously increased dramatically, corresponding to broadband acceleration processes that dominate the energy fluxes. This conclusion is supported by performed experiments, e. g. plotting the data for the less intense intermediate pitch angles (e. g. downward 120°-150°), which moves partially saturated spectra away from saturation while retaining the basic configuration shown in Figure 4 (albeit with less contrast): inverted-V's before and after the center of the event, and broadband distributions in the center. We have also seen a nearly identical repeat of the Figure 4 feature during Juno perijove 10 (PJ10; 1654-5 UT, 16 December 2017), with lower, unsaturated intensities (but also with poorer sampling in pitch angle).

It is significant that the upward-directed ion beams in Figure 4 occur only in association with the coherent electron acceleration. Within the broadband electron acceleration region, the ions become dimmer and also peak at intermediate pitch angles (panel 3D) suggestive of an ion conic (as observed elsewhere at Jupiter; Clark et al., 2017a), with a broad, falling energy distribution extending to several hundred keV. This conic-like distribution could be associated with perpendicular wave-particle energization followed by magnetic mirror force acceleration along the magnetic field, as is observed to happen at Earth (reviewed Pashmann et al., 2002 or Amm et al., 2002). Also for this case (as compared with Figure 1) there are much clearer examples of upward directed proton energy beams associated with the coherent downward accelerated electron beams (Spectra 9 and 10 in Figure 5; see the top of panel 4E for the time positions). The occurrence of strongly peaked up-going ion spectra is interpreted here as indicating that a fraction of the magnetic field-aligned electric potential resides below the spacecraft, as observed at Earth (Pashmann et al., 2002 or Amm et al., 2002). However, for this jovian example, the peaked distributions occur only sporadically, not continuously.

Transitions that have some superficial similarities to the one identified near the peak of the electron inverted-V in Figure 4 have been observed at Earth. These Earth transitions occur when the spacecraft moves from within the middle of the electric potential drop to being completely below it (Strangeway et al., 1998; Pashmann et al., 2002 or Amm et al. 2002). There, at Earth, the electron distributions broaden below the peaked electron energy, and there also appear conic ion distributions. But what is distinct about the Jupiter example is the high energy tail in the broadband regions, which would be observable both within and below a potential-driven acceleration region if the cause were similar to that causing the transitions at Earth. This high energy tail compels us to conclude that the cause of the transition at Jupiter is distinct from the cause of the superficially similar transitions at Earth.

5. Downward proton inverted-V

We turn now to the other feature of interest in Figure 3, the proton inverted-V structure on the left (panel 3G). This ion feature is most distinct in the downward direction (panel 3G) but is still quite present, if somewhat broadened, for ions measured in the perpendicular direction (panel 3F; Spectra 3 and 4 in Figure 5). The ion beam feature disappears completely only for the up-going directions (panels 3D and 3E), specifically when the sensors are looking down into the loss cone (estimated at this time as ~27°, again using the simple expression in Mauk et al., 1917a). At the same time as the observation of this high energy proton inverted-V there was observed a lower energy proton population (~30 keV; not shown). That population will be the subject of future studies in collaboration with the Juno plasma investigation (Jupiter Auroral Distributions Experiment; JADE; McComas et al., 2017).

We interpret this proton inverted-V feature as being a consequence of a downward-directed magnetic field aligned electric field with a total potential drop of 300 kV. Within other main auroral crossings, downward ion beams with inferred potentials up to >400 kV have been observed; eight clean main-aurora examples have been observed over nine Juno orbits. Within the polar cap, poleward of the main auroral oval, downward ion inverted-V structures have previously been reported (Clark et al.; 2017b) with inferred electric potentials of sometimes over a megavolt.

The fact that the signatures of the ion inverted-V downward electric potential occurs in both the downward and perpendicular directions to the magnetic field suggests that these potentials occur at significant distances anti-planetward from the spacecraft. As the accelerated ion beams move planetward, magnetic mirror forces will broaden the beams in angle such that some nearly field-aligned velocity vectors at high altitudes become

perpendicular at very low altitudes. However, because the downward ion energy beams have not been observe at radial distances >4 R_J over the main aurora (12 auroral crossings examined over 3-16 R_J radial positions), wave scattering could also play a role.

What is most interesting about these proton inverted-V structures within the main auroral oval (contrary to what is observed in the polar cap by Clark et al., 2017b) is that they can occur at the same position where there are huge downward electron energy fluxes sufficient to power the most intense auroras seen at Jupiter (both upward and downward acceleration is observed; see 3B). The presence of a broad, seemingly stable, down-going ion inverted-V makes it unlikely that there was a down-going electron inverted-V that was somehow involved with the broadband electron acceleration. This conclusion is based on the association of inverted-V's (at Earth) with up-going or down-going electric currents (Paschmann et al., 2002; Amm et al., 2002), each of which can generate only up-going or down-going electric fields, but not both. It would seem unlikely that these broadband electrons (Spectra 1 and 2 in Figure 5) started with a downward coherent (electric potential-driven) electron acceleration that became unstable. We note that for any one example of downward proton inverted-Vs, scenarios can be concocted whereby the source of the coherently accelerated ions is in the opposite hemisphere. However, such scenarios become nearly impossible to sustain over the record of observations from nine Juno science orbits.

6. Discussion

The two focus features of this study support the previous conclusion that broadband, perhaps stochastic, electron acceleration is responsible for the most intense auroras at Jupiter. However, coherent acceleration via magnetic field-aligned electric potentials can also contribute substantially; the electric potentials associated with our downward electric inverted-V delivered a substantial 1000 mW/m^2, but still below the >3000 mW/m^2 delivered

by the adjacent broadband acceleration. That downward electron inverted-V feature lends support to the previous speculation that electric potential-driven aurora can turn into broadband acceleration, perhaps by the initiation of an instability as the auroral drivers intensify; due to the intensification of a current, of the strength of the potential, or of some other relevant parameter. Note that while the feature looks spatial in character, it is possible that the transition occurred temporally rather than spatially. The above described process may indeed happen, but the other feature studied here makes it unlikely that such a process is necessary to the generation of all strong broadband downward acceleration. In that case the magnetic field-aligned electric potential appears to be in the wrong direction, downward rather than upward. The downward electron broadband acceleration, with energy flux values as high as have been observed at Jupiter, seem to have happened despite the presence of magnetic field aligned potentials rather than because of them. This latter feature is not just quantitatively different than observations at Earth; it has no known precedent at Earth.

We have yet to discover the causes of the broadband acceleration that is clearly so critical to generating Jupiter's uniquely powerful aurora. Stochastic processes occur at Earth (Pashmann et al., 2002 or Amm et al., 2002) but their characteristics appear different than those at Jupiter (Mauk et al., 2017a; 2017b). Achieving such understanding will require multi-instrument studies that include, in addition to JEDI, magnetic field perturbations (MAG, Connerney et al., 2017b), plasmas (JADE, McComas et al., 2017), plasma and radio waves (Waves, Kurth et al., 2017), and auroral imaging (UVS, Gladstone et al., 2017; JIRAM, Adriani et al., 2017). The JADE instrument (Jupiter Auroral Distributions Experiment) is of particular interest in that it allows for the extension of the particle observations down to much lower energies (ions ~5 eV to 50 keV and electrons 100 eV to 100 keV). Such particles are likely to be critically involved in the generation of the waves that accelerate the particles.

Acknowledgements. We are grateful to NASA and contributing institutions that played critical roles in making the Juno mission possible. We are grateful to JHU/APL's Lawrence E. Brown for his role in developing the core of the data display software used here, and JHU/APL's Donald G. Mitchell for providing insight into the energetic particle measurements in extremely harsh environments. This work was funded by NASA's New Frontiers Program for Juno via subcontract with the Southwest Research Institute. The data presented here are, or soon will be, available from the Planetary Plasma Interactions Node of NASA's Planetary Data System (https://pds-ppi.igpp.ucla.edu/). Access to analysis tools are available by contacting the lead author.

References

Adriani, A. et al. (2017), JIRAM, the Jovian Infrared Auroral Mapper, Space Sci. Rev., 213, Iss. 1-4, pp 393-446, doi:org/10.1007/s11214-014-0094-y.

Allegrini, F. et al. (2017), Electron beams and loss cones in the auroral regions of Jupiter, Geophys. Res. Lett., 44, doi:10.1002/2017GL073180.

Amm, O. et al. (2002), Chapter 4-In Situ Measurements in the Auroral Plasma, Space Science Reviews (2002) 103: 93. doi:10.1023/A:1023082700768 (2002).

Arnoldy, R. L. (1981),, Review of auroral particle precipitation, in Physics of Auroral Arc Formation, Geophys. Monogr. Ser., edited by Akasofu, S.-I., and J. R. Kan, vol. 25, p. 56., AGU, Washington, D. C., doi:10.1029/GM025.

Bagenal, F., Adriani, A., Allegrini, F. et al. (2014), Magnetospheric Science Objectives of the Juno Mission, Space Sci Rev, 213, Iss. 1-4, pp 219-287, doi:10.1007/s11214-014-0036-8.

Bolton et al. (2017a), The Juno mission, Space Sci. Rev., 213, Iss. 1-4, pp 5-37, doi:org/10.1007/s11214-017-0429-6

Bolton, J. S. et al. (2017b), Jupiter's interior and deep atmosphere: The initial pole-to-pole passes with the Juno spacecraft, Science, 356, 6340, 821-825.

Bonfond, B., et al. (2017), Morphology of the UV aurorae Jupiter during Juno's first perijove observations, Geophys. Res. Lett., 44, doi:10.1002/2017GL073114 (2017).

Clark, G., et al. (2017a), Observation and interpretation of energetic ion conics in Jupiter's polar magnetosphere, Geophys. Res. Lett., 44, 4419–4425, doi:10.1002/2016GL072325.

Clark, G., et al. (2017b), Energetic particle signatures of magnetic field-aligned potentials over Jupiter's polar regions, Geophys. Res. Lett., 44, 8703–8711, doi:10.1002/2017GL074366.

Connerney, J. E. P., M. H. Acuña, N. F. Ness, and T. Satoh (1998), New models of Jupiter's magnetic field constrained by the Io flux tube footprint, J. Geophys. Res., 103(A6), 11929–11939, doi:10.1029/97JA03726.

Connerney, JEP, et al. (2017a), Jupiter's magnetosphere and aurorae observed by the Juno spacecraft during its first polar orbits, Science, 356, 6340, 826-832, doi:10.1126/science.aam5928.

Connerney, J.E.P., Benn, M., Bjarno, J.B. et al. (2017b), The Juno magnetic field investigation, Space Sci Rev., 213, Iss. 104, pp 39-138, doi:10.1007/s11214-017-0334-z (2017).

Gladstone, G.R., Persyn, S.C., Eterno, J.S. et al. (2017), The Ultraviolet Spectrograph on NASA's Juno Mission, Space Sci Rev, 213, Iss. 1-4, pp 447-473, doi:10.1007/s11214-014-0040-z

Gérard, J.-C., B. Bonfond, D. Grodent, A. Radioti, J. T. Clarke, G. R. Gladstone, J. H. Waite, D. Bisikalo, and V. I. Shematovich (2014), Mapping the electron energy in Jupiter's aurora: Hubble spectral observations, J. Geophys. Res. Space Physics, 119, 9072–9088, doi:10.1002/2014JA020514.

Hess, S. L. G., B. Bonfond, P. Zarka, and D. Grodent (2011), Model of the Jovian magnetic field topology constrained by the Io auroral emissions, J. Geophys. Res., 116, A05217, doi:10.1029/2010JA016262.

Gustin, J., D. Grodent, L. C. Ray, B. Bonfond, E. J. Bunce, J. D. Nichols, N. Ozak (2016), Characteristics of north jovian aurora from STIS FUV spectral images, Icarus, 268, p. 215, doi:10.1016/j.icarus.2015.12.048.

Kurth, W. S., et al. (2017a). The Juno Waves investigation, Space Sci. Rev., 213, Iss. 1-4, pp 347-392, doi: 10.1007/s11214-017-0396-y.

Mauk, B. H., and N. J. Fox (2010), Electron radiation belts of the solar system, J. Geophys. Res., 115, A12220, doi:10.1029/2010JA015660.

Mauk, B. H. (2015), Comparative investigation of the energetic ion spectra comprising the magnetospheric ring currents of the solar system, J. Geophys. Res. Space Physics, 119, 9729–9746, doi:10.1002/2014JA020392.

Mauk, B. H., et al. (2017a), Juno observations of energetic charged particles over Jupiter's polar regions: Analysis of monodirectional and bidirectional electron beams, Geophys. Res. Lett., 44, 4410–4418, doi:10.1002/2016GL072286.

Mauk, B. H. et al. (2017b), Discrete and broadband electron acceleration in Jupiter’s powerful aurora, Nature, 549, 66, doi:10:1038/nature23648.

Mauk, B.H., Haggerty, D.K., Jaskulek, S.E. et al. (2017c), The Jupiter Energetic Particle Detector Instrument (JEDI) Investigation for the Juno Mission, Space Sci Rev, 213, Iss. 1-4, pp. 289-346, doi:10.1007/s11214-013-0025-3

McComas, D.J., Alexander, N., Allegrini, F. et al. (2017), The Jovian Auroral Distributions Experiment (JADE) on the Juno Mission to Jupiter, Space Sci Rev, 213, Iss. 1-4, pp 547-643, doi:10.1007/s11214-013-9990-9.

Paranicas, C., et al. (2017), Radiation near Jupiter detected by Juno/JEDI during PJ1 and PJ3, Geophys. Res. Lett., 44, 4426–4431, doi:10.1002/2017GL072600.

Paschmann, et al. (2002), Chapter 4-In Situ Measurements in the Auroral Plasma , Auroral Plasma Physics, Space Sciences Series of ISSI (International Space Sciences Institute), AIP-Press, ISBN 978-94-007-1086-3.

Strangeway et al. (1998), FAST observations of VLF waves in the auroral zone: Evidence of very low plasma densities, Geophys. Res. Lett., 25, No. 12, 2065-2068, doi:10.1029/98GL00664.

Zombeck, M. V. (2007), Handbook of Space and Astrophysics, 3rd Addition, , ISBN-13: 978-0521782425. Cambridge University Press, United Kingdom.

Figure Captions

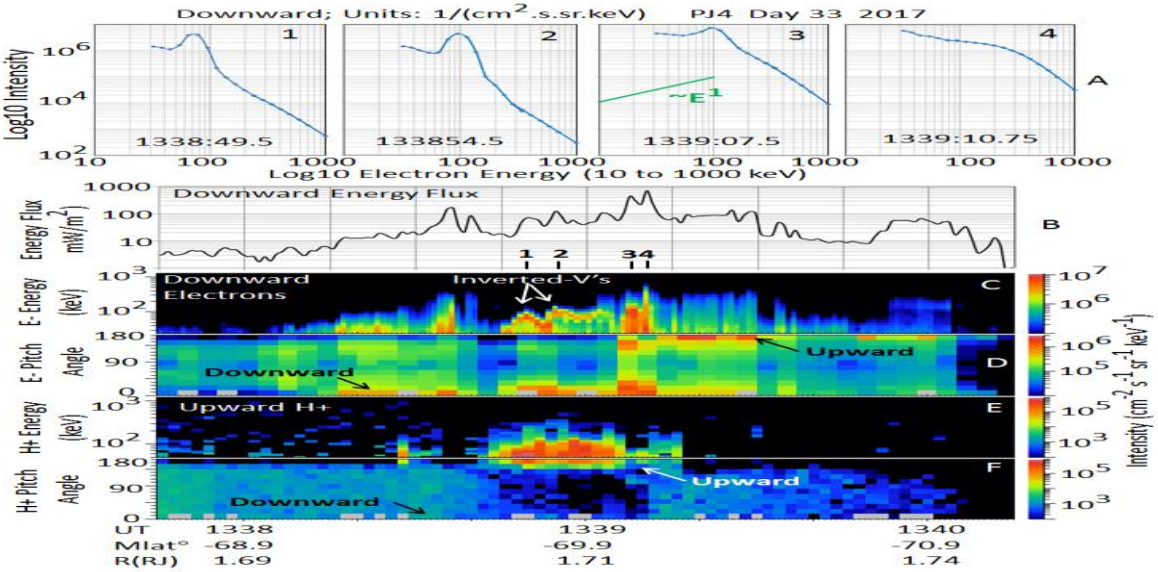

Figure 1. Selected energetic particle measurements obtained at low altitudes over Jupiter's main southern aurora on 2 February (Day 33) 2017 (modified from Mauk et al., 2017b, in Nature). A) Selected downward energetic electron energy spectra (differential number intensity) for pitch angles (PA) <30°. The selected times are identified panel B, bottom. B) Downward electron energy fluxes estimated as a minimum for > 30 keV electrons using the procedure identified in Mauk et al. (2017a; see also Supporting Information S2). C) Downward electron energy-time spectrograms (PA<30°) with intensity coded as color. D) Electron pitch angle distributions in the form of a differential intensity averaged over energies between 30 and 1000 keV. Pitch angles (angles between particle velocities and the local magnetic field direction) are calculated using measured magnetic fields from the MAG instrument (Connerney et al., 2017). E) Upward (PA >150°) proton energy spectra coded as color with an energy-time spectrogram format. F) Proton pitch angle distributions in the form of a differential intensity averaged over energies between 50 and 1000 keV. The magnetic latitude and L values shown here and elsewhere on the bottom of the plots were calculated using the dipole component of the VIP4 magnetic field model (Connerney et al., 1998).

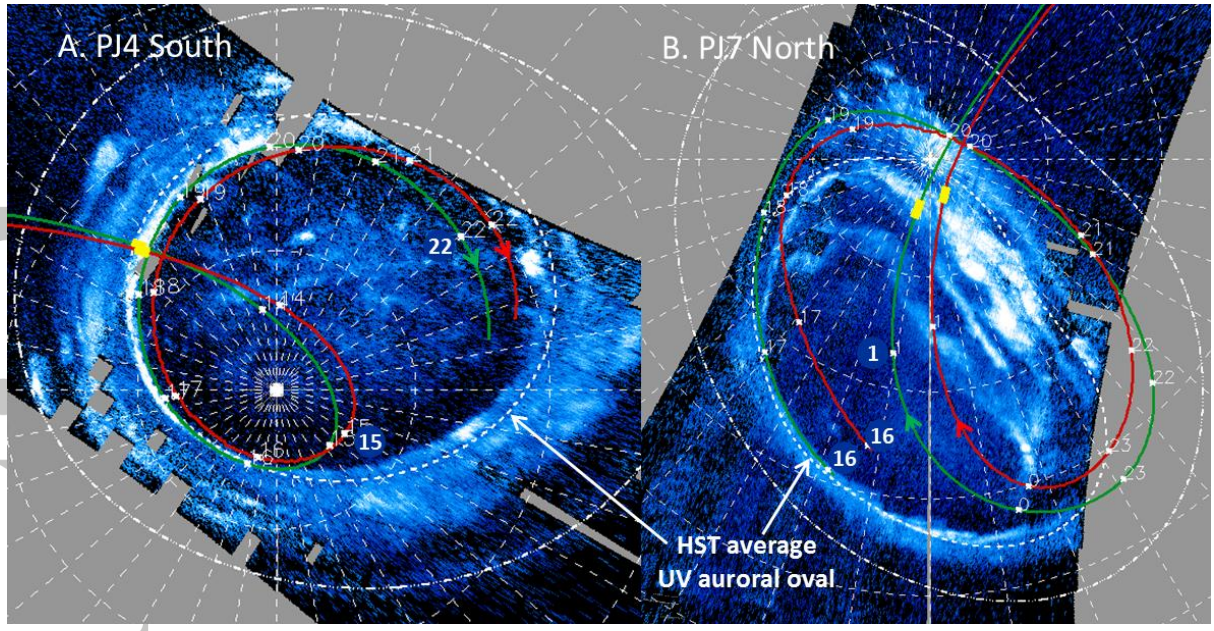

Figure 2. Juno observed ultraviolet images of Jupiter's auoral regions as measured by the Juno Ultraviolet Spectrograph (UVS) instrument (Gladstone et al., 2017). These false-color images, with a linear scale that is proportional to the overall UV intensities contain magnetic projections of Juno's position onto Jupiter's polar atmosphere calculated using pre-Juno magnetic field models (red and green for VIP4 from Connerney et al., 1998, and VIPAL from Hess et al., 2011). White dots on the trajectories show hours in UT, labeled occasionally with white numbers. Yellow markings on the trajectories in panels A and B correspond to the time periods of Figures 1 and 3, respectively. A) A southern auroral image obtained during perijove 4 (PJ4) on 2 February 2017. B) A northern auroral image obtained during PJ7 on 11 July 2017. Because the magnetic field models were generated prior to the Juno mission, there is a great deal of uncertainty in exactly to where the Juno trajectories map, as discussed more fully in the Methods section in Mauk et al., (2017b).

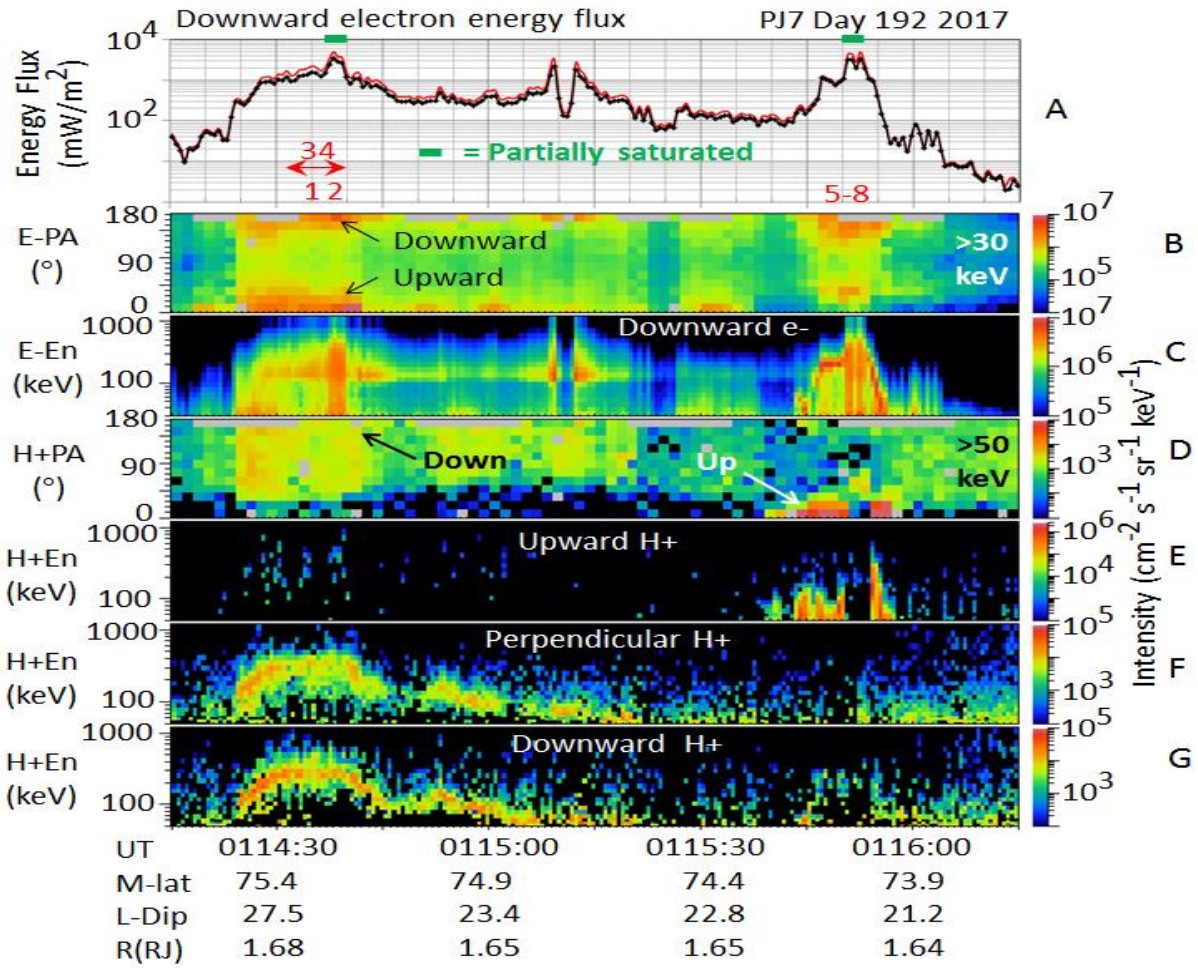

Figure 3. Selected energetic particle measurements obtained at low altitudes over Jupiter's main northern aurora on 11 July (Day 192) 2017. A) Downward electron energy fluxes calculated two different ways (see text and Supporting Information S2). . B) Electron pitch angle distributions (see Figure 1 details). C) Downward electron energy spectra. D) Proton pitch angle distributions for >50 keV protons. E) Energy spectrogram for >50 keV protons for protons with upward pitch angles between 0 and 30 degrees. F) Energy spectrogram for >50 keV protons with perpendicular pitch angles between 70 and 110 degrees. G) Energy spectrogram for >50 keV protons with downward pitch angles between 150 and 180 degrees.

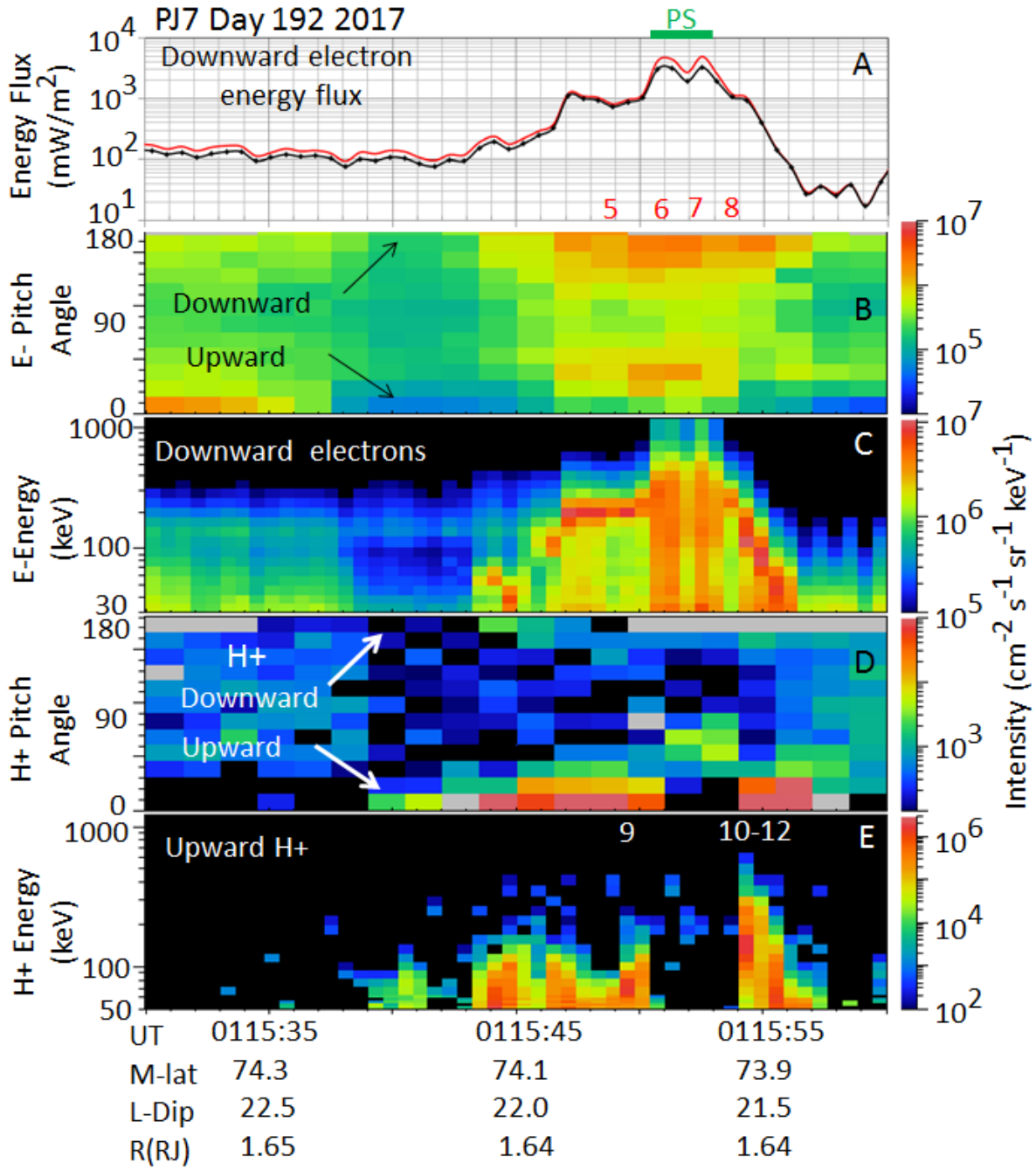

Figure 4. Detailed look at a portion of the time period shown in Figure 3 for panels A-E

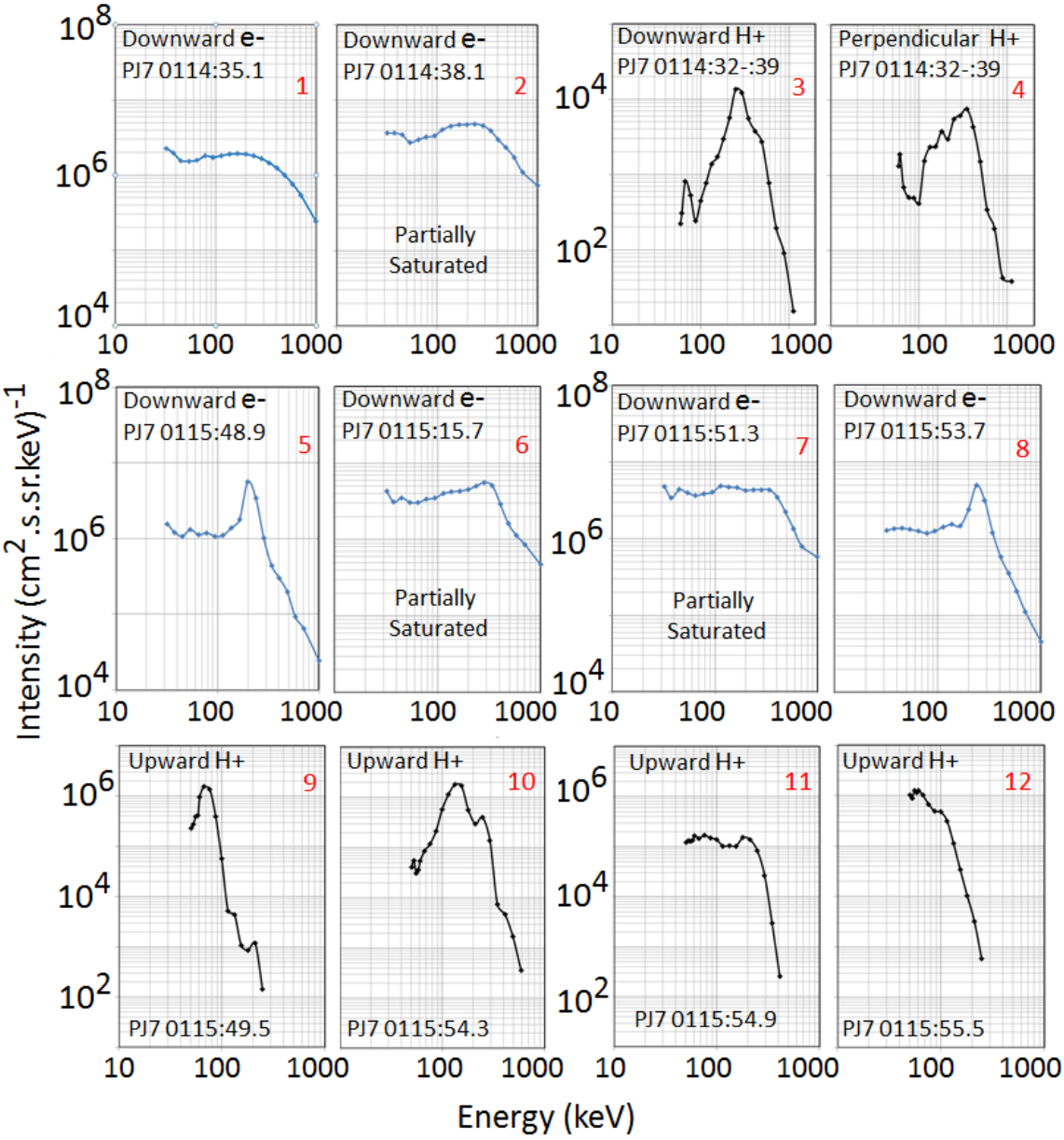

Figure 5. Selected electron (blue) and proton (black) number flux energy spectra sampled at selected times in Figures 3 and 4. The electron spectra have been corrected where needed for penetrators according to the procedures in the Supporting Information S1. The times associated with each spectra are identified by number at the bottom of panel A in Figure 3; and at the bottom of panel A in Figure 3 for electrons, and the top of panel E in Figure 4.